Power quality assessment of a wave energy converter using energy storage

Md Imran Ullah, Johan Forslund, Jessica S. Döhler and Irina Temiz

***Abstract*—Wave energy has been an immense area of interest in research and industry in our move toward a sustainable energy production society due to its high energy density and surface area. However, the grid connection of wave energy converters is still one of the major challenges due to the complexity of varying wave resources (amplitude and frequency). Wave energy converter grid integration can lead to several potential challenges, such as voltage fluctuations, harmonics and flicker. Using an energy storage system can help mitigate a few challenges by balancing the grid demand with the wave energy converter power supply. Hence, improving the power quality. This study assesses the power quality of wave energy converters equipped with energy storage against the scenario without any energy storage at different power levels. The power quality in this paper is investigated using total harmonic distortion (THD) of the grid current, dc-link voltage ripple and battery current ripple. The study shows that the addition of a hybrid energy storage system lowers the grid current THD at the point of common coupling (PCC), stabilizes the dc-link voltage ripple and reduces the stress of the battery.**

***Index Terms*—Wave energy converter, power quality, hybrid energy storage system, grid following control, battery, supercapacitor.**

I. Introduction

In comparison to well-established renewable energy sources like wind and solar energy, harnessing electrical energy from the ocean waves is one of the relatively recent additions to renewable energy technologies. The emergence of this particular form of energy can be traced back to the oil crisis of 1973, which sparked significant interest in exploring alternative energy options. By the year 1980, a considerable number of patents had already been filed, demonstrating the growing enthusiasm and recognition of the technological possibilities associated with wave energy [1].

Wave energy is considered a secondary form of energy as it is generated through the continuous interaction of wind with the ocean's surface, and winds are generated by the uneven heating of the Earth's surface caused by solar energy. The average annual wave energy density (50 kW/m) [2] is higher than that of its counterpart wind energy $(500\ W/m^2 - 1000\ W/m^2)$ [3] in global wind-rich areas with less on average variability. It is estimated that wave energy has a theoretical potential of around 80,000 Twh [4]. However, wave energy poses certain disadvantages due to its inherently destructive nature and variability. One of the major disadvantages of the wave energy converter is its variability which varies across different time scales (wave to wave, different sea states, seasonal variation) [1].

Wave energy harnessing devices can be categorized according to their design and their principle of harnessing energy. A few notable categories are oscillating water columns, overtopping systems, attenuators and point absorbers [5]. This paper discusses Uppsala University's developed wave energy converter (WEC) [6]. This system is a permanent magnet linear synchronous generator-based wave energy converter. The translator of the generator is directly connected to the buoy, which constitutes its power take-off (PTOs). This connection has been identified as the optimal choice and is called direct drive PTOs [7]. Due to the inherent variability in wave amplitude and frequency, the grid connection of a direct drive-based linear generator PTOs has several potential challenges, such as voltage fluctuations and harmonics, voltage stability issues, voltage flicker at the PCC [8], and weak grids arise when connecting the WEC to the grid [9].

Several approaches are being employed to enhance the power quality, such as using an energy storage system [10] [11], wave prediction [12], reactive power compensation [13], and WEC placement strategy [14]. The concept of aggregating several WECs into a WEC farm leads to a reduction of average power variability has been studied in [15]. However, this concept can make the power quality of the wave farm susceptible to destructive wave interactions and also doesn't allow the control of the power flow to the grid.

Energy storage, such as the battery [11], superconducting magnetic storage system [16], mechanical energy storage system [17], and supercapacitor [18] etc.

Part of a special issue for EWTEC 2023. Original version published in EWTEC 2023 proceedings at https://doi.org/10.36688/ewtec-2023-315.

Manuscript submitted 17 December 2024; Accepted 13 January 2025. Published 31 May 2025.

This paper has been subjected to single-blind peer review by a minimum of two reviewers.

This work was supported in part by the STandUP for Energy.

Md. Imran Ullah is a PhD student at Uppsala University, Department of Electrical Engineering, Ångströmlaboratoriet, Lägerhyddsvägen 1, 75237 Uppsala, Sweden (e-mail: imran.ullah@angstrom.uu.se).

Johan Forslund is an assistant professor at Uppsala University, Department of Electrical Engineering, Ångströmlaboratoriet, Lägerhyddsvägen 1, 75237 Uppsala, Sweden (e-mail: johan.forslund@angstrom.uu.se).

Jessica S. Döhler is a PhD student at Uppsala University, Department of Electrical Engineering, Ångströmlaboratoriet, Lägerhyddsvägen 1, 75237 Uppsala, Sweden (e-mail: jessica.santos@uu.se).

Irina Temiz is an associate professor at Uppsala University, Department of Electrical Engineering, Ångströmlaboratoriet, Lägerhyddsvägen 1, 75237 Uppsala, Sweden (e-mail: irina.temiz@angstrom.uu.se).

Digital Object Identifier: https://doi.org/10.36688/imej.8.57-63

is being used for mitigating the power variations of a single WEC or a wave farm. These energy storage systems can successfully reduce variability and enable control over the power flow to the grid, depending on the control of their energy management systems. Nevertheless, there is still limited research regarding the quantified impact of energy storage systems on the power quality of grid-tied WECs.

The current study investigates, compares and quantifies the power quality of the WEC at different grid input power levels equipped with no HESS, with the usage of just a battery and with both a battery and supercapacitor. The study assesses the power quality of a single wave energy converter grid connection by analyzing the parameters such as THD of the grid current, which according to grid code standard IEEE 519-2022, must be lower than 5%, and also the dc-link voltage ripple and the battery current ripple. Grid-following (GFL) control is used for the grid-side three-phase IGBT-based(insulated-gate bipolar transistor) inverter. Active and reactive power control is used for the scenario equipped with HESS, and dc-voltage control is used for the scenario without HESS [19]. The study shows that using an energy storage system reduces wave farm optimization design dependency and enhances power quality at the PCC.

The paper is organized as follows: Section 2 is divided into five parts, including wave energy system description, linear generator, proposed system, grid-forming control and hybrid energy storage system control. Section 3 discusses the simulation setup, which includes wave climate and load selected to test the WEC and the electrical network. Section 4 presents and discusses the simulated results from MATLAB/Simulink. Section 5 concludes the paper by summarizing the findings and their implications for future research.

II. Methodology

A. Linear generator-based wave energy converter

This section briefly discusses the WEC model and the linear generator. For detailed modelling, the reader can refer to [20], [21] and [22].

The linear generator is placed on the seabed, and the buoy is at the water's surface. The translator of the generator is connected to the buoy via a connection line. The WEC system can be seen in Fig. 1.

The heave motion of the buoy lifts the translator, and the gravitational force pulls it down. The governing equations for the motion of the buoy and the translator are given [20]

$$m_b\ddot{z}_b(t) = F_{gb} + F_{wb}(t) + F_b + F_e(t) + F_r(t) + F_{hs}(t) \quad (1)$$

and

$$m_t\ddot{z}_t(t) = F_{gt} + F_{PTO}(t) + F_{wt}(t) + F_{es}(t), \quad (2)$$

where m_b, m_t are the mass of the buoy and translator; $\ddot{z}_b(t)$, $\ddot{z}_t(t)$ are the accelerations of the buoy and translator correspondingly; F_{gb}, F_{gt} are the gravitational forces on the buoy and translator; F_b is the buoyancy force; $F_e(t)$ is the excitation force; $F_r(t)$ is the radiation force; $F_{hs}(t)$ is the hydrostatic restoring force; $F_{PTO}(t)$ is the damping force of the PTO; $F_{es}(t)$ is the end-stop force; $F_{wb}(t)$ and $F_{wt}(t)$ are the wire force for the buoy and the translator, respectively. An illustration of different forces on the buoy and translator can be seen in Fig. 2.

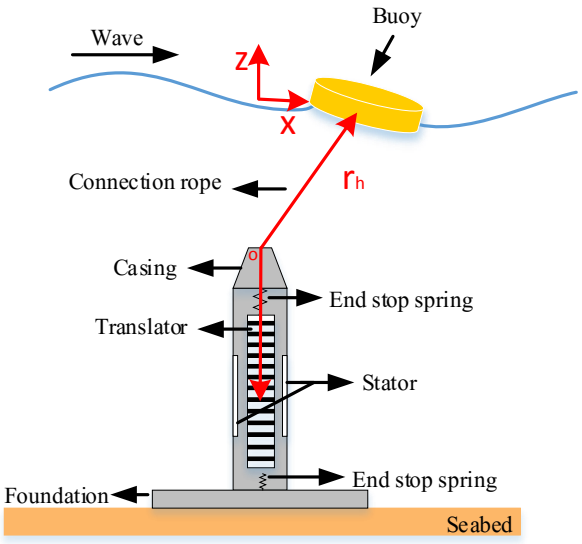

Fig. 1. Wave energy converter [22].

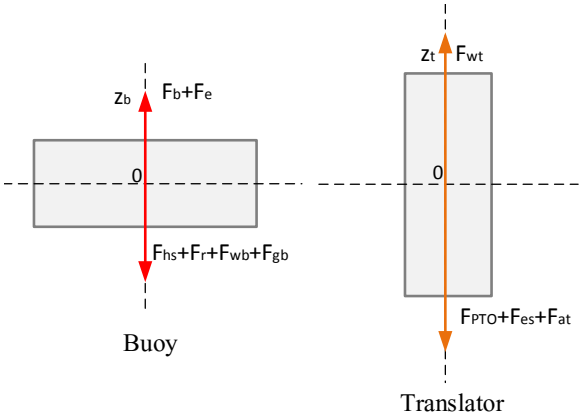

Fig. 2. Forces on the buoy and the translator [22].

The generator is a permanent magnet direct-drive linear generator. It is modelled using a single-phase equivalent circuit for a non-salient generator. Magnetic flux is given by

$$\Phi = \Phi_0 \cos(\frac{2\pi}{\tau_p} z_t(t) + \psi) \quad (3)$$

where Φ_0 is the amplitude of the magnetic flux, τ_p is the pole pair width, $z_t(t)$ is the translator displacement, and ψ is the phase shift, $\psi = 0, \pm 2\pi/3$. The generator induced emf e is calculated from

$$e = -N\,\frac{\mathrm{d}\Phi}{\mathrm{d}t} = E_p \sin(\frac{2\pi}{\tau_p} z_t(t) + \Phi) \quad (4)$$

where $Ep = 2\pi N \Phi_0 \dot{z}_t/\tau_p$ is the amplitude of no-load voltage, and N is the total number of turns of the stator windings.

B. Proposed system description

The proposed system consists of a linear generator-based wave energy converter connected to a strong utility grid. The generator-side converter is a diode-based three-phase passive rectifier that is connected to a dc-link capacitor. The HESS is connected at the dc-link via non-isolated bi-directional dc/dc converters. The HESS consists of a battery and supercapacitor, which is responsible for low-frequency and high-frequency power fluctuations originating from the single WEC, respectively. The grid-side converter is a three-phase IGBT-based inverter that is connected to the grid via an L filter at the PCC. Fig. 3 shows a general schematic of a wave power plant connected to a grid using an energy storage system. In the absence of energy storage, neither a supercapacitor nor a battery is present.

C. Control implementation

Three different scenarios of grid-connected WEC with and without energy storage systems are implemented. The cascade control method is used for all the scenarios, which implies the use of two control loops. The outer control loop provides the set point for the inner control loop.

- **Case 1**: Without energy storage. No energy storage system is used in this scenario. The dc-link voltage is controlled by the converter, which provides the reference for the inner control loop. The grid-side converter is used to balance the dc bus voltage. Hence, all available power from the WEC will be directly injected into the grid without a predetermined set point for grid power injection.
- **Case 2**: Battery energy storage. The battery controls the dc-link voltage, which provides the reference for the battery's inner control loop. The grid-side converter controls the current set according to the power demand from the grid. In this scenario, the battery is balancing the dc-link voltage.
- **Case 3**: Battery and supercapacitor energy storage. Both a battery storage system and a supercapacitor will be utilized. The supercapacitor is responsible for controlling the dc-link voltage, which provides the reference for both the battery and supercapacitor current loop. In this scenario, the hybrid energy storage system is balancing the dc-link voltage. A low-pass filter (LPF) is used to segregate the high-frequency power fluctuations from the low-power fluctuations from the WEC. The supercapacitor is used to smooth out the high-frequency fluctuations, whereas the battery is responsible for low frequency.

1) Current control (Case 1): To derive the inner current control loop, the three-phase equations for grid-connected converters can be written using Kirchhoff's voltage law

$$\begin{cases} L\frac{\mathrm{d}i_a(t)}{\mathrm{d}t} = v_{t,a}(t) - ri_a(t) - v_a(t) \\ L\frac{\mathrm{d}i_b(t)}{\mathrm{d}t} = v_{t,b}(t) - ri_b(t) - v_b(t) \\ L\frac{\mathrm{d}i_c(t)}{\mathrm{d}t} = v_{t,c}(t) - ri_c(t) - v_c(t), \end{cases} \tag{5}$$

where $v_a(t)$, $v_b(t)$ and $v_c(t)$ are the three-phase voltages at the PCC, $v_{t,a}(t)$, $v_{t,b}(t)$ and $v_{t,c}(t)$ are the voltages at the terminal of the converter. The output filter is represented by r and L. Referring to Fig. 4, a two-phase dq synchronous reference frame model of the voltage source converter is

$$\begin{cases} L\frac{\mathrm{d}i_d(t)}{\mathrm{d}t} = L\omega i_q(t) + v_{t,d}(t) - ri_d(t) - v_d(t) \\ L\frac{\mathrm{d}i_q(t)}{\mathrm{d}t} = -L\omega i_d(t) + v_{t,q}(t) - ri_q(t) - v_q(t). \end{cases} \tag{6}$$

The proposed cascade PI controller sets a voltage reference V_{dc}^* for the outer voltage control loop. The outer loop gives the inductor reference current i_d^* for the inner current loop, while the inner loop provides the index modulation m_d and m_q for the pulse width modulation, as can be seen in Fig. 4 when the switch is connected to port 1.

The feedback control loop of the inner current control, which has a plant $P(s) = \frac{1}{Ls+r}$, is combined with a PI controller $C_d(s) = C_q(s) = k_{p,i}\frac{s+\frac{k_{i,i}}{k_{p,i}}}{s}$. The equation of the closed loop is compared with the first-order equation $F(s) = \frac{1}{\tau_i s+1}$ in order to find the gains of the control, resulting in

$$\begin{aligned} k_{p,i} &= \frac{L}{\tau_i} \\ k_{i,i} &= \frac{r}{\tau_i}. \end{aligned} \tag{7}$$

For a quick response, $\frac{1}{\tau_i}$ has to be at least 10 times smaller than the switching frequency. Due to that, a time constant of 0.5ms was used [19].

2) dc-link voltage control (Case 1): Voltage control on the dc-link takes into account the power balance between the dc-link bus at the capacitor and the AC power grid [19]

$$\frac{C_{eq}}{2}\frac{\mathrm{d}v_{dc}^2(t)}{\mathrm{d}t} = P_{in}(t) - \frac{3}{2}v_{t,d}(t)i_d(t), \tag{8}$$

where C_{eq} is capacitance, voltage, v_{dc} is the voltage at the capacitor, $P_{in}(t)$ is the power injected by the WEC.

The feedback control loop of the outer voltage control, which can be seen in Fig. 4 when the switch is connected to port 1, has a plant $V(s) = \frac{-3v_d}{C_{eq}s}$, is combined with a PI controller $C_{vdc}(s) = k_{p,v}\frac{s+\frac{k_{i,v}}{k_{p,v}}}{s}$. The equation of the closed loop is compared with the second-order equation $G(s) = \frac{2\xi\omega_n s+\omega_n^2}{s^2+2\xi\omega_n s+\omega_n^2}$ in order to find the gains of the control, resulting in

$$\begin{aligned} k_{p,v} &= \frac{2\xi\omega_n C_{eq}}{3v_d} \\ k_{i,v} &= \frac{\omega_n^2 C_{eq}}{3v_d}. \end{aligned} \tag{9}$$

The natural frequency $\omega_n = 2\pi \times 15$ rad/s and the damping ratio $\xi = 0.707$ is decided for this paper. The parameter values for the converter and the inner and outer control loops are given in Table I.

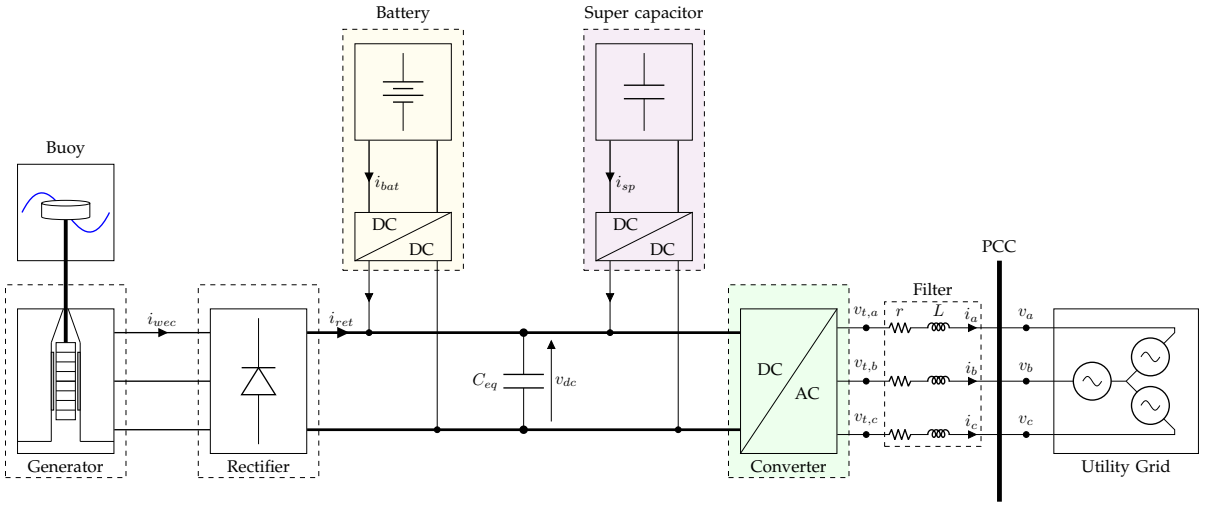

Fig. 3. Grid connected WEC system.

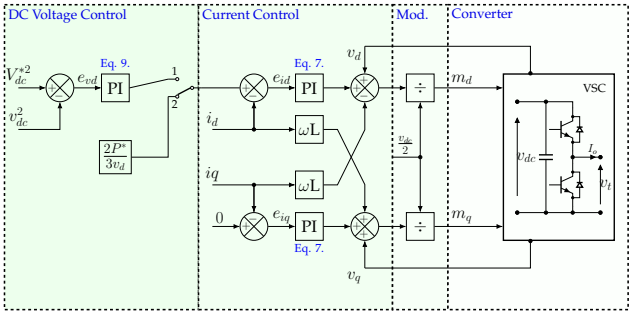

Fig. 4. Block diagram of the grid following inverter control.

TABLE I
PARAMETERS OF THE GRID-CONNECTED CONVERTER.

Parameter	Value
Nominal voltage (V_{rms})	220 V
Switching frequency	20 kHz
Nominal frequency	50 Hz
L filter	r = 0.3Ω and L = 2 mH
Nominal dc voltage	600 V
dc-link filter	C_{eq} = 5500 μF
Current loop gains	$k_{p,i}$ = 4 and $k_{i,i}$ = 600
dc voltage loop gains	$k_{p,v}$ = 0.3629 and $k_{i,v}$ = 24.42

3) Current control (Case 2 and Case 3): Fig. 5 illustrates the control strategy implemented in the HESS of a grid-tied WEC. Non-isolated bi-directional dc/dc converters are employed to charge or discharge the supercapacitor and the battery banks according to the proposed control.

The dc-link bus voltage (v_{dc}) is controlled by the voltage control loop. It then generates the inner loop current reference for the supercapacitor. From Fig. 5, Kirchhoff's current law is used to represent the outer voltage control loop which results in the following differential equation

$$i_{sp}(t) = i_{dc}(t) + \frac{\mathrm{d}C_{eq}v_{dc}(t)}{\mathrm{d}t} \tag{10}$$

The feedback control loop of the voltage control, which has a plant $D(s) = \frac{1}{C_{eq}s}$, is combined with a

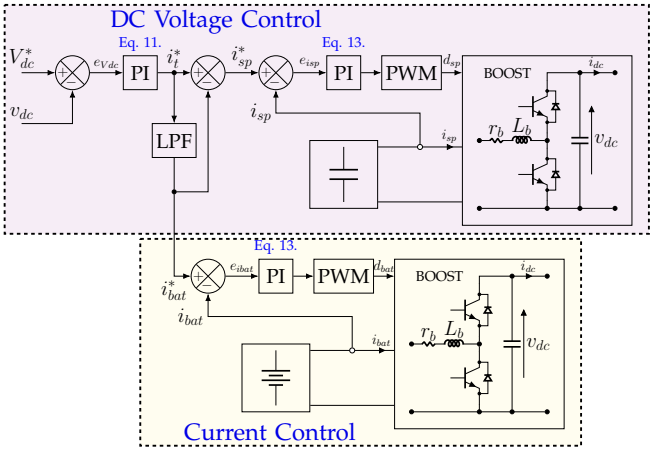

Fig. 5. Block diagram of voltage and current control for HESS.

PI controller $C_v(s) = k_{p,vdc}\frac{s+\frac{k_{i,vdc}}{k_{p,vdc}}}{s}$. The equation of the closed loop is compared with the second-order equation $F(s) = \frac{2\xi_{dc}\omega_{ndc}s+\omega_{ndc}^2}{s^2+2\xi_{dc}\omega_{ndc}s+\omega_{ndc}^2}$, which are

$$\begin{aligned} k_{p,vdc} &= 2\xi_{dc}\omega_{ndc}C_{eq} \\ k_{i,vdc} &= \omega_{ndc}^2 C_{eq}, \end{aligned} \tag{11}$$

where $\omega_{ndc} = 2\pi \times 128$ rad/s and $\xi_d = 0.707$.

Supercapacitors and battery control loops are similarly modelled. In Equation (13), the letter m and n are used to represent the battery and the supercapacitor, respectively. From Fig. 5, Kirchhoff's voltage law is used to model the internal current control, which derives the following differential equation

$$L_{m,n}\frac{\mathrm{d}i_{m,n}(t)}{\mathrm{d}t} + r_{m,n}i_{m,n}(t) = v_{m,n}(t) - v_{t_{m,n}}(t), \tag{12}$$

where $v_{t_{m,n}}(t)$ is the terminal voltage, $v_{m,n}(t)$ is the battery and supercapacitor voltage, $i_{m,n}(t)$ is the battery and supercapacitor current, $L_{m,n}(t)$ is the inductor filter and $r_{m,n}$ is the internal resistance of the filter. The pulse-width modulation (PWM) is used by the converter as a control strategy. Hence, $v_{t_{m,n}} = d_{m,n}(t)\, v_{dc}(t)$.

Referring to Fig. 4, connecting the switch to port 2 provides the reference current for the current control. The reference current depends on the instantaneous active power (P^*) demand by the grid. The feedback control loop of the current control, which has a plant $T(s) = \frac{1}{L_b s + r_b}$, is combined with a PI controller $C_b(s) = C_c(s) = k_{p,imn}\frac{s+\frac{k_{i,imn}}{k_{p,imn}}}{s}$. The equation of the closed loop is compared with the first-order equation $H(s) = \frac{1}{\tau_{imn}s+1}$. The PI controller gains are

$$\begin{aligned} k_{p,imn} &= \frac{L_{m,n}}{\tau_{im,in}} \\ k_{i,imn} &= \frac{r_{m,n}}{\tau_{im,in}}. \end{aligned} \tag{13}$$

where $\tau_{im} = 0.32$ms and $\tau_{in} = 0.16$ms. The dynamic behaviour of the battery and supercapacitor decides their current control loop design, which is based on the dc/dc converter switching frequency. The control loop of the battery's current is designed to be slower compared to the supercapacitor due to its inherently faster charge and discharge rates.

The higher-frequency sinusoidal currents are primarily smoothened out by supercapacitor instead of the battery. Fig. 5 illustrates the outer control voltage loop, which regulates the dc-link voltage and then provides the total current reference i_t^*. The reference is then divided into two different components. The low-frequency component i_{bat}^* is for the battery's dc/dc converter. The high-frequency component i_{sp}^* is for the supercapacitor's dc/dc converter. The transient components are allocated to the supercapacitor with higher power density with the help of LPF, whereas the remaining average component is received by the battery. A cut-off frequency of 50 Hz has been selected in this study. Table II provides the parameter values for the converter, as well as the inner and outer loop control gains.

TABLE II
PARAMETERS OF THE HESS CONTROLLER.

Parameter	Value
Nominal voltage supercapacitor	300 V
Switching frequency	25 kHz
L filter	r_c = 0.03 Ω and L_c = 4 mH
Supercapacitor capacity	R.volt = 5.5 V, R.cap = 1 F
	Eq.res= 0.5 Ω, N.cells = 55
Current loop gains	$k_{p,ic}$ = 25 and $k_{i,ic}$ = 187.5
dc voltage loop gains	$k_{p,vc}$ = 6.29 and $k_{i,vc}$ = 3.6 10^3
Nominal voltage battery	340 V
Switching frequency	25 kHz
L filter	r_b = 0.03 Ω and L_b = 4 mH
Battery capacity	R.volt = 3.6 V, R.bat = 9 Ah
	Eq.res = 0.12 Ω, N.cells = 95
Current loop gains	$k_{p,ib}$ = 12.5 and $k_{i,ib}$ = 93.75

III. SIMULATION SETUP

The power quality of the system will be assessed through a series of simulations conducted under different sea states. Key parameters such as the THD of the grid current, the voltage ripple at the dc bus, and the dc current ripple to the battery will be recorded to evaluate the power quality.

A. Wave climate and electrical system topology

To investigate the impact of different sea states on the system, the WEC will be subjected to different excitation forces. The model is simulated for initial 2 seconds, with a peak power of 67 kW and an average power of 37.2 kW, see Fig. 6. Specifically, a time duration from 1.2 to 1.4 seconds in the WEC power, highlighted by dashed lines in the figure, will be analyzed to assess power quality. To analyze the influence of the battery and supercapacitor on power quality, three different system configurations will be considered, which have been discussed in Section II-C.

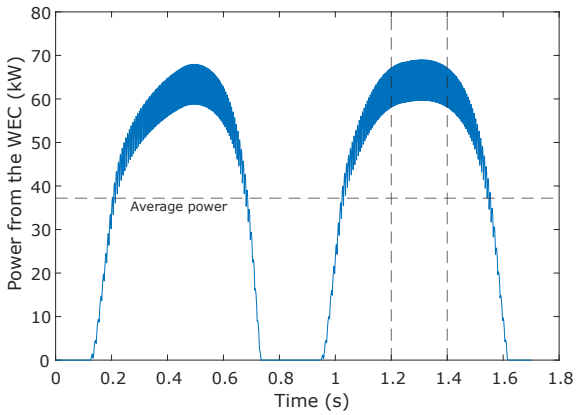

Fig. 6. Power from the WEC during the high sea state, used as input for the electrical system. Average WEC power is marked with a horisontal dashed line. The time span for analysis is marked with vertical dashed lines.

B. Selection of data for analysis

For each case, a range of set points (2, 5, 10, 15, 20, 30, 40 and 48 kW) will be employed to determine the active power injected into the grid. The battery size has been chosen to ensure a constant injected active power as dictated by the set point.

In order to conduct an accurate analysis of harmonic content, a sufficient number of periods is necessary. However, due to variations in the current amplitude during each WEC power cycle, the accuracy of THD calculations is compromised. To enhance accuracy, fewer cycles will be used for analysis, albeit at the expense of lower resolution. Specifically, five cycles will be employed for analysis.

As the battery charge current fluctuates during operation, the ripple of the current will also change. To calculate the ripple factor of the battery charge current, a time interval from 1.3 to 1.333 seconds has been chosen to represent the charge current.

IV. RESULTS

In order to comply with grid standards, it is necessary for the THD of the grid current to be below 5%. This study aims to investigate the impact of various energy storage configurations (no storage, battery-only, or battery with a supercapacitor) on the THD of the grid current, as well as the ripple voltage at the dc bus and the ripple of the battery charge current.

Simulations have been conducted for different levels of injected power into the grid, using the WEC power profile depicted in Fig. 6. By varying the injected d-axis current, the injected active power is adjusted from 2 kW to 50 kW.

In the case of no energy storage, all available power from the WEC is directly injected into the grid. As shown in Fig. 7, the THD exhibits an inverse relationship with the injected power. Notably, without energy storage, the THD remains consistently higher for lower injected power and fails to meet the 5% grid standard. The THD meets the 5% grid standard with the increment of injected power. However, when a battery is employed, along with the inclusion of a supercapacitor, the THD remains unchanged. At the lowest set point, the THD is slightly above 5%, but decreases to 0.25% at 48 kW injected power.

Fig. 8 illustrates the voltage ripple of the DC bus. Without energy storage, the ripple is measured at 0.56% for low power and decreases to 0.1% for the highest power level. The inclusion of a battery reduces the ripple to 0.04%, but increases with higher power levels to 0.1%. Incorporating a supercapacitor leads to a greater ripple, consistently at 0.09% independent of power level. The supercapacitor controls the dc link voltage in the case of HESS control. The supercapacitor has a faster charge, discharge rate and low energy compared to the battery, leading to a slightly higher ripple at the dc bus voltage.

Examining the ripple of the battery charge current, as displayed in Fig. 9, reveals the impact of using only a battery or combining a battery with a supercapacitor. The data demonstrate that adding a supercapacitor reduces the ripple across the entire range of injected power. The supercapacitor substantially reduces the ripple factor for low power, from 1.28% to 0.09%, and for high power, from 36.08% to 1.36%, resulting in a reduction of the ripple factor by a factor of 14-26. The data shows that the current ripple while using a supercapacitor is less dependent on the injected power.

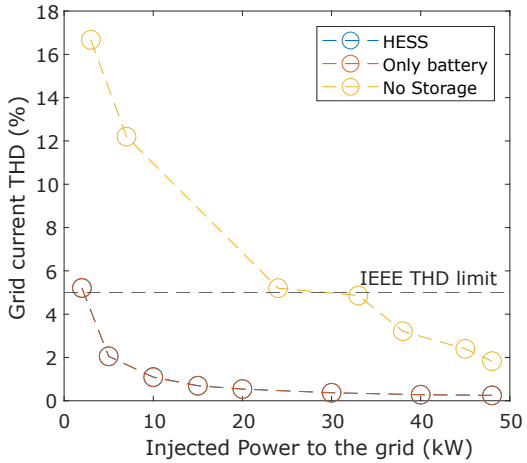

Fig. 7. Calculated THD of the grid current for the three simulated cases: No storage, only battery storage, and HESS.

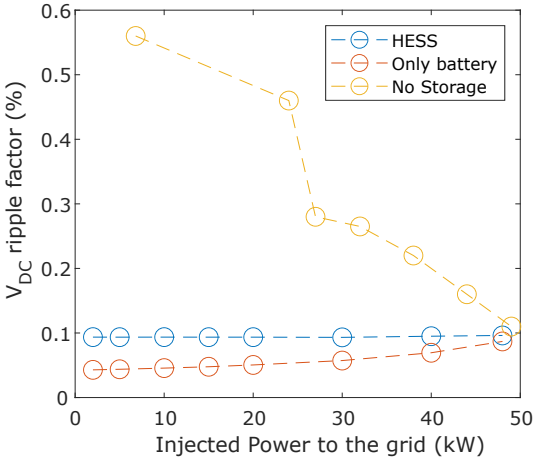

Fig. 8. Calculated ripple of the dc bus voltage for the three simulated cases: No storage, only battery storage, and HESS.

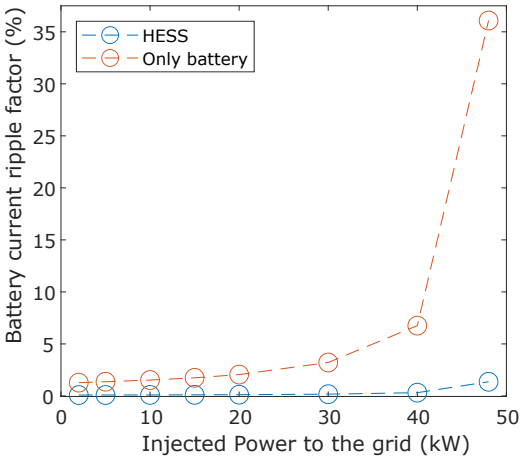

Fig. 9. Calculated ripple of the battery current for two of the simulated cases: Only battery storage, and HESS.

V. Conclusion

Simulations of a range of injected power to the grid have been conducted for three cases: No storage, a battery storage, and a combination of battery and supercapacitor. The power quality analysis focuses on the THD of the grid current, the ripple of the dc bus voltage, and the ripple of the battery charge current. Without an energy storage, the THD of the grid current only meets the grid code requirement IEEE 519-2022 of below 5% for high power injected to the grid. Introducing a battery significantly reduces the THD of the grid current, enough to fulfill the requirement for all injected power except very low levels. The battery also heavily reduces the ripple factor of the DC bus voltage. To reduce stress on the battery, the use of a supercapacitor effectively decreases the ripple of the charge current by a factor of 14-26, and also allows the battery current ripple to be less dependent on the injected power. However, it should be noted that the introduction of a supercapacitor also increases the voltage ripple on the DC bus, but the impact is less at higher power. This is because the supercapacitor has a much faster charge, discharge rate and low energy

compared to the battery, leading to a slightly higher ripple at the dc bus voltage. In absolute numbers, the voltage ripple factor is still very low, 0.56% without energy storage and below 0.1% for the either battery or HESS.

ACKNOWLEDGEMENT

The author would like to thank Uppsala University (Sweden), STandUP for Energy, and Åforsk travel grant for their financial support.

REFERENCES

[1] A. F. d. O. Falcão, "Wave energy utilization: A review of the technologies," *Renewable and sustainable energy reviews*, vol. 14, no. 3, pp. 899–918, 2010.

[2] A. M. Cornett, "A global wave energy resource assessment," in *The Eighteenth international offshore and polar engineering conference*. OnePetro, 2008.

[3] C. wei Zheng and J. Pan, "Assessment of the global ocean wind energy resource," *Renewable and Sustainable Energy Reviews*, vol. 33, pp. 382–391, 2014.

[4] S. Anttila, D. Silva, I. Temiz, J. G. d. Oliveira, J. Leijon, A. Parwal, and C. Boström, "Power control strategies for a smoother power output from a wave power plant," in *13th European Wave and Tidal Energy Conference (EWTEC), Napoli, Italy, September 1-6, 2019*. European Wave and Tidal Energy Conference, 2019.

[5] B. Drew, A. R. Plummer, and M. N. Sahinkaya, "A review of wave energy converter technology," 2009.

[6] A. Parwal, F. Remouit, Y. Hong, F. Francisco, V. Castelucci, L. Hai, L. Ulvgård, W. Li, E. Lejerskog, A. Baudoin *et al.*, "Wave energy research at uppsala university and the lysekil research site, sweden: A status update," in *Proceedings of the 11th European Wave and Tidal Energy Conference. Nantes, France, September 2015*, 2015.

[7] N. J. Baker, "Linear generators for direct drive marine renewable energy converters," Ph.D. dissertation, Durham University, 2003.

[8] A. Blavette, D. L. O'Sullivan, A. W. Lewis, and M. G. Egan, "Impact of a wave farm on its local grid: Voltage limits, flicker level and power fluctuations," in *2012 Oceans-Yeosu*. IEEE, 2012, pp. 1–9.

[9] H. A. Said and J. V. Ringwood, "Grid integration aspects of wave energy—overview and perspectives," *IET Renewable Power Generation*, vol. 15, no. 14, pp. 3045–3064, 2021.

[10] M. I. Ullah, J. S. Döhler, D. C. Silva Júnior, C. Boström, J. G. Oliveira, and I. Temiz, "Analysis of a hybrid energy storage system in a grid-tied wave energy converter for varying power demand," in *11th International Conference on Renewable Power Generation - Meeting net zero carbon (RPG 2022)*, vol. 2022, 2022, pp. 218–222.

[11] A. Parwal, J. Hjalmarsson, T. Potapenko, S. Anttila, J. Leijon, J. Kelly, I. Temiz, J. G. de Oliveira, C. Boström, and M. Leijon, "Grid impact and power quality assessment of wave energy parks: Different layouts and power penetrations using energy storage," *The Journal of Engineering*, vol. 2021, no. 8, pp. 415–428, 2021.

[12] G. Li, G. Weiss, M. Mueller, S. Townley, and M. R. Belmont, "Wave energy converter control by wave prediction and dynamic programming," *Renewable Energy*, vol. 48, pp. 392–403, 2012.

[13] J. Sjolte, G. Tjensvoll, and M. Molinas, "All-electric wave energy converter array with energy storage and reactive power compensation for improved power quality," in *2012 IEEE Energy Conversion Congress and Exposition (ECCE)*. IEEE, 2012, pp. 954–961.

[14] M. Neshat, B. Alexander, and M. Wagner, "A hybrid cooperative co-evolution algorithm framework for optimising power take off and placements of wave energy converters," *Information Sciences*, vol. 534, pp. 218–244, 2020.

[15] M. Giassi and M. Göteman, "Layout design of wave energy parks by a genetic algorithm," *Ocean Engineering*, vol. 154, pp. 252–261, 2018.

[16] Z. Nie, X. Xiao, Q. Kang, R. Aggarwal, H. Zhang, and W. Yuan, "Smes-battery energy storage system for conditioning outputs from direct drive linear wave energy converters," *IEEE Transactions on Applied Superconductivity*, vol. 23, no. 3, pp. 5 000 705–5 000 705, 2013.

[17] Q. Gao, B. Ding, N. Ertugrul, and Y. Li, "Impacts of mechanical energy storage on power generation in wave energy converters for future integration with offshore wind turbine," *Ocean Engineering*, vol. 261, p. 112136, 2022.

[18] D. B. Murray, M. Egan, J. Hayes, and D. O'Sullivan, "Applications of supercapacitor energy storage for a wave energy converter system," in *EWTEC 2007-7th European Wave and Tidal Energy Conference*, 2009.

[19] A. Yazdani and R. Iravani, *Voltage-sourced converters in power systems: modeling, control, and applications*, 1st ed. Hoboken: John Wiley & Sons, 2010.

[20] W. Chen, I. Dolguntseva, A. Savin, Y. Zhang, W. Li, O. Svensson, and M. Leijon, "Numerical modelling of a point-absorbing wave energy converter in irregular and extreme waves," *Applied Ocean Research*, vol. 63, pp. 90–105, 2017.

[21] I. Dolguntseva, S. Eriksson, and M. Leijon, "Electrical approach to output power control for a point absorbing wave energy converter with a direct drive linear generator power take off," in *Proceedings of the 12th European Wave and Tidal Energy Conference*. Cork, Ireland, 2017, p. 878.

[22] T. Potapenko, J. Burchell, S. Eriksson, and I. Temiz, "Wave energy converter's slack and stiff connection: Study of absorbed power in irregular waves," *Energies*, vol. 14, no. 23, p. 7892, 2021.